Journal of Computational Physics 228 (2009) 881–902

Contents lists available at ScienceDirect

Journal of Computational Physics

journal homepage: www.elsevier.com/locate/jcp

A priori mesh quality estimation via direct relation between truncation error and mesh distortion

Y. Kallinderis *, C. Kontzialis

Laboratory for Aerodynamic Design of Air Vehicles, Department of Mechanical and Aeronautical Engineering, University of Patras, Panepistimioupoli, 26504 Rio, Greece

ARTICLE INFO

Article history:
Received 10 May 2008
Received in revised form 24 July 2008
Accepted 3 October 2008
Available online 25 October 2008

Keywords:
Field simulations
Grid quality
Truncation error
Grid distortion
Hybrid mesh
Finite volume method

ABSTRACT

The purpose of the present work is the derivation and evaluation of *a priori* mesh quality indicators for structured, unstructured, as well as hybrid grids. Emphasis is placed on deriving direct relations between the indicators and mesh distortion. The work is based on use of the finite volume discretization for evaluation of first order spatial derivatives. The analytic form of the truncation error is derived and applied to elementary types of mesh distortion including typical hybrid grid interfaces. The corresponding analytic expressions provide direct relations between computational accuracy and the degree of stretching, skewness, shearing and non-alignment of the mesh.

1. Introduction

The drive for field simulations that incorporate complex physics and geometries poses a formidable challenge to grid generation [1]. The distribution of points and elements can be quite non-uniform and coarse leading to inaccurate computations. The inaccuracy is often assessed after the simulation is performed causing repetitive grid generations and subsequent field simulations. It is desirable to have an assessment of the appropriateness (quality) of the mesh before performing the simulation.

Grid quality is affected by two primary factors; the local size of the computational elements, and the uniformity of the spatial distribution of the points/elements. A primary method for solving the issue of coarse mesh resolution has been adaptive refinement [2–6]. While substantial work has been performed on this type of mesh adaptation, relatively less work has been devoted to study and improvement of the local distribution of the points, which basically relates to the shape of the elements. The present work focuses on this contributor to the error. Assessment of adequacy of local resolution and shape of the elements depends on the discretization error. It is imperative to derive measures of this error in the computation.

Two broad categories of error indicators are: (i) *a priori* and (ii) *a posteriori* estimation. The two approaches are basically complimentary. *A priori* error evaluation can aid in mesh generation, while *a posteriori* can provide guidance to mesh adaptation techniques during the simulation. The present work falls under the first class, which does not make use of the field solution. Previous work bases the *a priori* grid quality assessment on geometric characteristics of the elements such as ratios of sizes of neighboring elements, as well as on element shape measures, such as angles and ratios of the radii of inscribed to

* Corresponding author.
E-mail addresses: kallind@otenet.gr (Y. Kallinderis), ckontzialis@lycos.com (C. Kontzialis).

0021-9991/$ - see front matter © 2008 Elsevier Inc. All rights reserved.
doi:10.1016/j.jcp.2008.10.023

prescribed circles [7–11]. In the Finite Element method, the quality of a mesh is often given in terms of the element/mesh regularity. This type of approach has given measures that can be computed easily and are quite popular with practical applications.

The present work also assesses grid quality by computing appropriate metrics of the elements. However, there are two distinguishing aspects of it: (i) the metrics indicating quality are derived *directly* from related analytic forms of the truncation error and (ii) can give analytic expressions for reducing the discretization error via re-shaping of the elements.

Truncation error (TE) analysis usually falls under the *a posteriori* estimation. The Finite Difference discretization method has offered a vehicle for calculating the TE via performance of *Taylor* series expansions of the solution at the points forming the discretization stencil [12]. The complexity of the expressions has led previous work to focus on simplified model field equations [13–15]. Nevertheless, those works expressed the strong dependence of the solution and the stability of the computations on the grid and its quality.

Direct relations between TE and mesh distortion parameters, such as departure from orthogonality and uniformity have been reported in [16,17]. Significantly less work exists for unstructured meshes [18] and for the finite volume (FV) method [19,20]. However, despite the large number of studies on the relation on the TE to the numerical solution, there have been very few derivations of mesh quality measures based on it.

The primary issue with TE analysis is the complexity of the related expressions, especially for multi-dimensions and for general hybrid mesh topologies. The present work addresses this complexity barrier via employment of symbolic mathematics software [21].

A posteriori error estimation methods include the *Richardson* extrapolation [22–25]. Use is made of two or more grids of the same domain with the difference in the yielded solution offering a measure of the local error distribution. Generating and solving on multiple meshes can be quite difficult for practical applications.

Another *a posteriori* method evaluates the error indirectly via tracking of the numerical solution variation (e.g. [26]). Local field features, such as boundary layers, shock waves and vortices are detected using sensors that are based on variations of the computed field parameters, such as the pressure and velocity. The assumption here is that the discretization error is large where the solution variations are large. The method has been primarily used for guiding grid adaptation. It is not a method that can directly yield practical assessment of grid quality, taking also into account that it necessitates expensive computations for large meshes and/or complex fields.

Another school of *a posteriori* error estimation work employs Finite Element discretization and derives analytic expressions of error bounds [27–30]. Various model equations have been utilized in order to provide the estimates. Although, the error bounds do not yield grid quality measures directly, there is potential for such use. Again, knowledge of the solution field is needed.

In Section 2 the analytic form of the TE in the evaluation of the first spatial derivatives is derived. The main types of mesh distortion are defined in Section 3, while Section 4 relates the TE and mesh distortion. In Section 5, the proposed mesh quality indices are presented, while Section 6 deals with their application to structured, unstructured and hybrid meshes.

2. Truncation error for hybrid meshes in two dimensions

The goal of the present work is the derivation of *a priori* quality measures for hybrid meshes. The most fundamental computation is that of first order derivatives. The first derivative is common not only to fluid flow governing equations, but also to other field equations. The relative reduced complexity of the related mathematics and its commonality led to its choice in the present work. The finite volume (FV) method will be the method of discretization. A central-type and node-based FV method is chosen as the vehicle for derivation of quality measures, since it is known to be sensitive to mesh non-uniformity in terms of its accuracy. The complete expressions for the TE will be presented for meshes that consist of structured, unstructured, or both types of elements. The complexity of the analytic expressions lead to study of the two-dimensional case, first.

A common FV evaluation of the first order spatial derivatives employs the *median* dual area around a grid point as 1 depicts [31,32]. This quite common FV evaluation is chosen to study quality measures. It is expected to reveal distortions of the

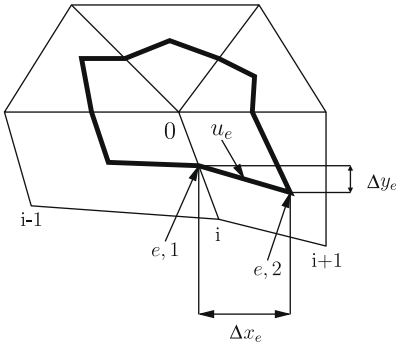

Fig. 1. *Median* dual surface for evaluating first order derivatives at grid point 0 via the finite volume method.

mesh as it corresponds to a central differencing and thus deemed sufficient for this study. The evaluation of the gradient ∇u is accomplished via the following contour integration:

$$\nabla u \approx \frac{1}{S}\oint_{\partial l} u d\boldsymbol{l} \approx \frac{1}{S}\sum_{e} u_e(\Delta y_e \hat{\boldsymbol{i}} - \Delta x_e \hat{\boldsymbol{j}}) \equiv \nabla^h u, \tag{1}$$

where S is the dual area, u_e is the field value at the middle of each edge of the dual contour, while Δx_e and Δy_e are the projections in the x- and y-direction of the edges of the dual contour joining the centroids of each element sharing point 0 with the middle of the grid edges sharing this point. This contour is termed *median dual* [31]. Other choices of dual surfaces include the surface formed by joining the centroids of the elements sharing point 0 (*centroid* dual), as well as the surface of the union of those elements.

Since the goal is deriving a quality measure the specific choice is not important. A node-based evaluation of the derivatives is considered, which will reveal the inaccuracy due to the distorted elements in a relatively straightforward manner.

2.1. The general form of the truncation error

The TE in the computation of the gradient is defined as:

$$\boldsymbol{E}(x,y) = \nabla^h u(x,y) - \nabla u(x,y), \tag{2}$$

with $\nabla^h u$ and ∇u being the numerical and the analytical values of the gradient, respectively. The analysis is similar in the x- and y-directions and employs *Taylor* series expansions for u^h at the required locations around point 0. The expansions are substituted into the TE definition of Eq. (2). The amount of operations involved is very large. This must have been one of the main reasons for not seeing complete TE analysis in previous works. In the present work the hurdle is overcome via use of the symbolic mathematics capability of Matlab [21].

The TE terms are grouped according to the following general form given for the case of evaluating the derivative in the x-direction (u^h_x):

$$E^x = e^x_x u_x + e^x_y u_y + e^x_{xy} u_{xy} + e^x_{xx} u_{xx} + e^x_{yy} u_{yy} + e^x_{xxx} u_{xxx} + e^x_{yyy} u_{yyy} + e^x_{xyy} u_{xyy} + e^x_{xxy} u_{xxy} + \ldots \tag{3}$$

The terms with the symbol e are functions of the metrics of the mesh and will be the vehicle for making the connection of the TE with mesh distortion. They will be termed *error coefficients* (EC). Their analytic expressions are grouped according to the order in terms of the local mesh size h.

The first two terms are involved in the consistency checks of the numerical approximation:

$$e^x_x = \frac{1}{2S}\sum_{e=1}^{n}(\Delta x_{e,1} + \Delta x_{e,2})\Delta y_e - 1, \tag{4a}$$

$$e^x_y = \frac{1}{2S}\sum_{e=1}^{n}(\Delta y_{e,1} + \Delta y_{e,2})\Delta y_e. \tag{4b}$$

The grid metrics involved in the above expressions are defined as follows:

$$(\Delta x_{e,k})^j(\Delta y_{e,k})^l = \frac{1}{N_{e,k}}\sum_{m=1}^{N_{e,k}}(x_m|_{e,k} - x_0)^j(y_m|_{e,k} - y_0)^l, \Delta y_e = y_{e,2} - y_{e,1}, \tag{5}$$

where $x_m|_{e,k}, y_m|_{e,k}$ and $N_{e,k}$ are the coordinates and the number of nodes participating in the averaging of u at the dual vertex $e,k(k=1,2)$. Generally, if a *median* dual vertex coincides with the middle point of an edge sharing point 0, then $N_{e,k}=2$, and *if* it coincides with the center of a quadrilateral or a triangle then $N_{e,k}=4$, or $N_{e,k}=3$, respectively. In Eq. (5) it is observed that the metric terms $\Delta x_{e,1}, \Delta x_{e,2}, \Delta y_{e,1}$ and $\Delta y_{e,2}$ are $O(h)$ each.

In the above expressions, n is the number of the dual edges, S is the dual area and it is $O(h^2)$, while $e,1$ and $e,2$ denote the end points of each edge of the dual contour, as shown in Fig. 1.

The next three terms are first order:

$$e^x_{xy} = \frac{1}{2S}\sum_{e=1}^{n}(\Delta x_{e,1}\Delta y_{e,1} + \Delta x_{e,2}\Delta y_{e,2})\Delta y_e, \tag{6a}$$

$$e^x_{xx} = \frac{1}{2S2!}\sum_{e=1}^{n}[(\Delta x_{e,1})^2 + (\Delta x_{e,2})^2]\Delta y_e, \tag{6b}$$

$$e^x_{yy} = \frac{1}{2S2!}\sum_{e=1}^{n}[(\Delta y_{e,1})^2 + (\Delta y_{e,2})^2]\Delta y_e. \tag{6c}$$

For the purpose of deriving quality measures, the second order terms are retained also:

$$e^x_{xxx} = \frac{1}{2S3!}\sum_{e=1}^{n}[(\Delta x_{e,1})^3 + (\Delta x_{e,2})^3]\Delta y_e, \tag{7a}$$

$$e^x_{yyy} = \frac{1}{2S3!}\sum_{e=1}^{n}[(\Delta y_{e,1})^3 + (\Delta y_{e,2})^3]\Delta y_e, \tag{7b}$$

$$e^x_{xyy} = \frac{1}{2S2!}\sum_{e=1}^{n}[\Delta x_{e,1}(\Delta y_{e,1})^2 + \Delta x_{e,2}(\Delta y_{e,2})^2]\Delta y_e, \tag{7c}$$

$$e^x_{xxy} = \frac{1}{2S2!}\sum_{e=1}^{n}[(\Delta x_{e,1})^2\Delta y_{e,1} + (\Delta x_{e,2})^2\Delta y_{e,2}]\Delta y_e. \tag{7d}$$

When the projections Δx_e and Δy_e are symmetrical relative to point 0, the computation becomes of second order and the TE expression reduces to the following:

$$\begin{aligned} E^x &= e^x_{xxx}u_{xxx} + e^x_{xyy}u_{xyy}, \\ E^y &= e^y_{yyy}u_{yyy} + e^y_{xxy}u_{xxy}. \end{aligned} \tag{8}$$

Meshes that give a TE form given in Eq. (8) will be termed *ideal* meshes. Orthogonal and equally-spaced in each direction quadrilaterals form an ideal mesh. The equivalent with triangles is an unstructured mesh with equal-length projections of their dual edges in the x- and y-directions. This definition will be used subsequently to define a quality measure.

Similar expressions for the EC regarding evaluation of the derivative in the y-direction hold. The projection Δy_e is replaced with Δx_e and a minus sign is placed in front of the sums. The EC e^y_x and e^y_y are given below:

$$e^y_x = -\frac{1}{2S}\sum_{e=1}^{n}(\Delta x_{e,1} + \Delta x_{e,2})\Delta x_e, \tag{9a}$$

$$e^y_y = -\frac{1}{2S}\sum_{e=1}^{n}(\Delta y_{e,1} + \Delta y_{e,2})\Delta x_e - 1. \tag{9b}$$

2.2. Consistency condition

A consistent discretization of the gradient requires the TE to vanish as the mesh size approaches zero. For zero mesh size all the EC become equal to zero, except for e^x_x, e^x_y in Eq. (4) and e^y_x, e^y_y in Eq. (9), and the TE in Eq. (2) becomes:

$$\begin{aligned} E^x &= e^x_x u_x + e^x_y u_y, \\ E^y &= e^y_y u_y + e^y_x u_x. \end{aligned} \tag{10}$$

It is noted that the EC $e^x_x, e^y_x, e^x_y, e^y_y$ remain unchanged for fixed-shape mesh elements even if the local mesh size is changing. For a consistent discretization, it is required that:

$$e^x_x = e^x_y = e^y_x = e^y_y = 0. \tag{11}$$

Following Eq. (11) the expressions of the EC e^x_x in Eq. (4) and e^y_y in Eq. (9) show that in order for them to vanish on a general mesh, the area evaluation of the following two expressions must yield the same result.

$$\begin{aligned} S_x &= \frac{1}{2}\sum_{e=1}^{n}(\Delta x_{e,1} + \Delta x_{e,2})\Delta y_e, \\ S_y &= -\frac{1}{2}\sum_{e=1}^{n}(\Delta y_{e,1} + \Delta y_{e,2})\Delta x_e. \end{aligned} \tag{12}$$

Using the *median* dual surface, from Eq. (12) it results that the two forms for evaluating the dual area produce the same result. Specifically, their difference is the following:

$$\sum_e [x_{e,2}y_{e,2} - x_{e,1}y_{e,1} - 2x_0(y_{e,2} - y_{e,1})] = 0, \tag{13}$$

and so $e^x_x = e^y_y = 0$ on a *hybrid* mesh. Carrying out the algebra in the expression of the EC e^x_y in Eq. (4)**?** using the *median* dual results:

$$e^x_y = \frac{1}{2S}\sum_e [y^2_{e,2} - y^2_{e,1} - 2y_0(y_{e,2} - y_{e,1})] = 0. \tag{14}$$

Analogously, the EC e^y_x in Eq. (9) results to be always zero on a *hybrid* mesh. So, the *median* dual surface leads to a consistent approximation of ∇u.

Using the *centroid* dual, from Eq. (12) it results that the two forms for evaluating the dual area do not produce the same result on *structured* meshes. Their difference considering a structured mesh is:

$$\frac{1}{8}\sum_i [x_i(y_{i+1}-y_{i-1})+y_i(x_{i+1}-x_{i-1})] \neq 0, \tag{15}$$

and so $e_x^x \neq 0, e_y^y \neq 0$ on a structured mesh. Carrying out the algebra in the expression of the EC e_y^x in Eq. (4) using the *centroid* dual it gives:

$$e_y^x = \frac{1}{8S}\sum_i [y_i(y_{i+1}-y_{i-1})] \neq 0. \tag{16}$$

Analogously, the EC e_x^y in Eq. (9) is not always zero on *structured* meshes. So, the consistency of the *centroid* dual depends on the geometry of a *structured* mesh in the approximation of ∇u.

Using the *centroid* dual, from Eq. (12) it results that the two forms for evaluating the dual area produce the same result on *unstructured* meshes. The difference of the two forms in Eq. (12) considering an unstructured mesh is:

$$\frac{1}{6}\sum_i [x_i(y_{i+1}-y_{i-1})+x_i(y_{i+1}-y_{i-1})] = 0, \tag{17}$$

and so $e_x^x = e_y^y = 0$ on unstructured meshes. Carrying out the algebra in the expression of the EC e_y^x in Eq. (4) using the *centroid* dual it gives:

$$e_y^x = \frac{1}{6S}\sum_i [y_i(y_{i+1}-y_{i-1})] = 0. \tag{18}$$

Analogously, the EC e_x^y in Eq. (9) is always zero on *unstructured* meshes. So, the *centroid* dual gives a consistent approximation of ∇u on *unstructured* meshes.

At *hybrid* mesh interfaces it is difficult to check analytically the consistency of the approximation of ∇u using the *centroid* dual. Despite this fact, it is anticipated that the computation will be inconsistent due to the inconsistency of the *centroid* dual expressions on structured meshes.

2.3. Verification of the error coefficients analytic expressions

It is of importance to check the complex expression of the TE using analytic field functions $u(x,y)$. The TE is computed by substituting the analytic values of the spatial derivatives and the values of the EC in Eq. (3). This will be termed the *analytic* TE. The TE is also computed *directly* by subtracting the analytic expression for ∇u from the FV expression $\nabla^h u$ Eq. (2). This second approach will be termed *numerical* TE.

Let us consider a field function $u(x,y)$, which resembles a boundary layer type of flow field with a linear variation in the streamwise direction:

$$u(x,y) = xy^2. \tag{19}$$

The differences between the *analytic* and the *numerical* TE values are calculated for the hybrid mesh of Fig. 2 using both the *median* and the *centroid* dual. A feature of this mesh is a local lateral displacement in the vicinity of an interface point. For the *median* dual the distribution of the *analytic* and the *numerical* TE is shown in Fig. 3. It is observed that the derived expressions are coincident within plotting accuracy.

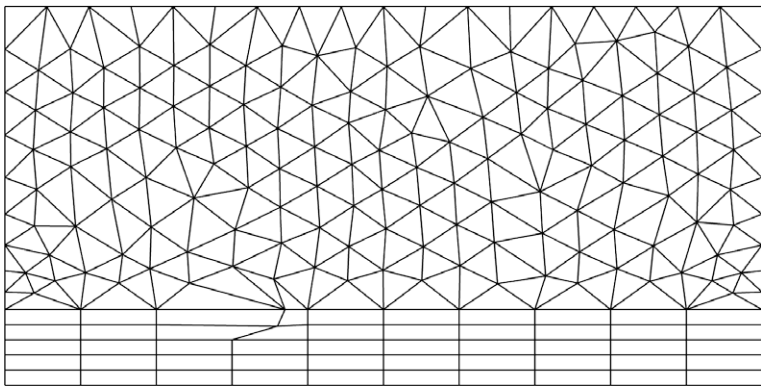

Fig. 2. *Hybrid* channel mesh.

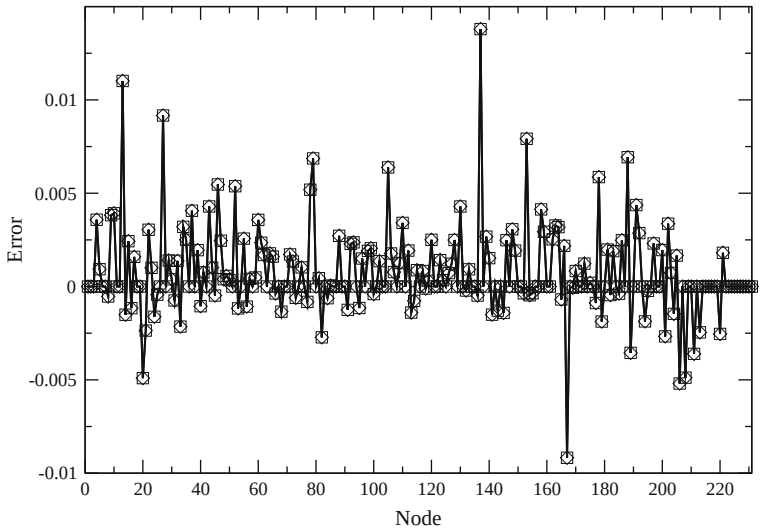

Fig. 3. Distribution of the analytic (□) and the numerical (◇) TE for the field $u(x,y) = xy^2$ on the mesh of Fig. 2 using the *median* dual.

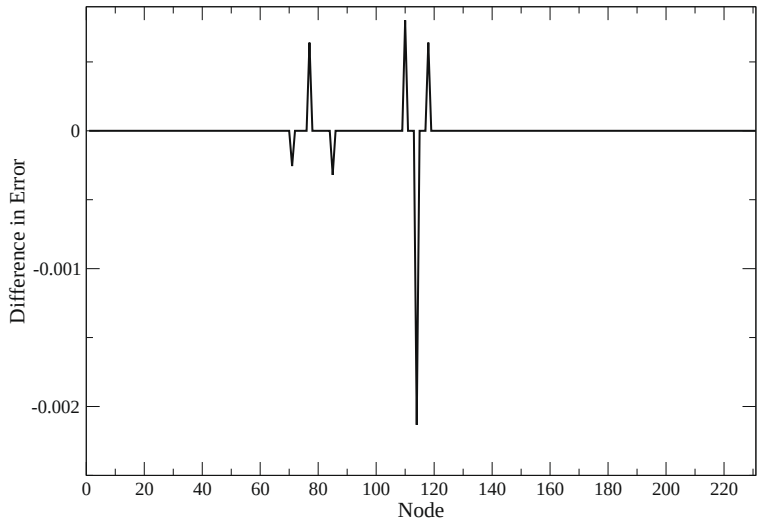

Fig. 4. Difference between the analytic and the numerical TE for the field $u(x,y) = xy^2$ on the mesh of Fig. 2 using the *centroid* dual.

Check of consistency "experimentally" via successive reductions of the size of the mesh elements may be impractical for large meshes. An indirect check of the consistency is proposed here by computing the difference between the *analytic* and *numerical* TE, without including in the analytic expression the error coefficients "responsible" for consistency (e_x^x and e_y^x). When including these terms, which are independent of the local mesh size, the difference will be zero within machine accuracy. If it is not, as the case is for the *centroid* dual discretization (see Fig. 4), a local inconsistency is revealed. The "spikes" in Fig. 4 correspond to points in the vicinity of the locally distorted mesh interface. The same inconsistency was revealed for the case of a distorted structured mesh.

Similar results were observed using other field functions, as well. This provides assurance that the derived complex expressions are correct. A further check of their validity, even though indirect, will be provided when checking the subsequently derived quality measures.

3. Elementary types of mesh distortion

The general mesh depicted in Fig. 1 exhibits skewness, stretching, offset of point 0 from the center of the control surface, as well as interfaces between structured and unstructured elements. It is important in the context of the present work to "isolate" each type of mesh "defect" and relate it *directly* to the TE. This is very important for future work on improving

the mesh during or immediately after its generation. Distortion types are easier to define on a quadrilateral mesh, compared to a triangular for which the offset of point 0 from the dual centroid is a reasonable measure. Regarding the interfaces between quadrilateral and triangular elements, three distinct types were identified and studied. It should be noted that skewness, stretching and center point offset are distortions that are not independent from each other. Application of one of them to an ideal mesh causes appearance of the rest. Nevertheless, this categorization offers a clear way to express the TE as a direct function of them and to come up with ways to reduce those distortions. It should be noted that the present work considers interior point configurations. Boundary "central" points (node 0 in Fig. 1) are not examined as the application of boundary conditions often "discards" the local discretization.

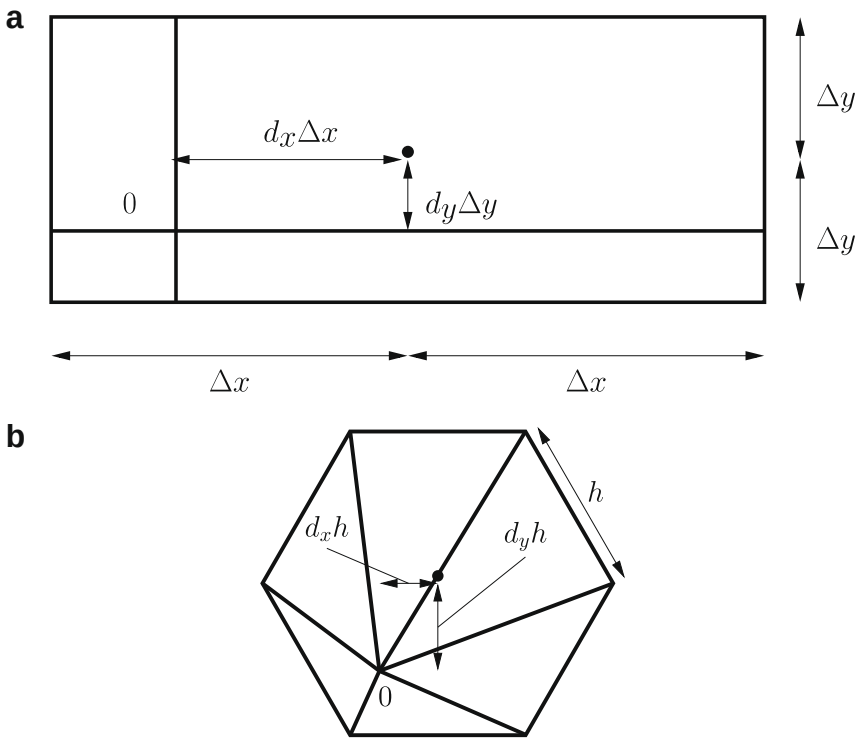

Fig. 5. Stretching for (a) structured and (b) unstructured meshes defined to facilitate comparison of accuracy degradation on them.

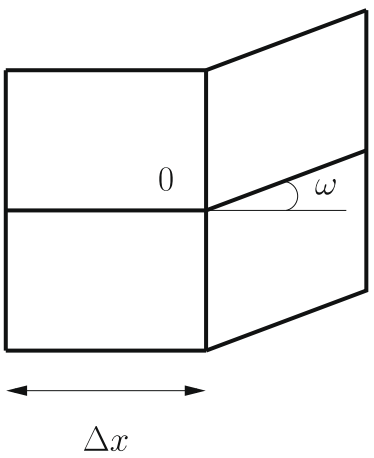

Fig. 6. *Skewed* mesh, depicting the deviation angle ω from the 180° angle between one of the two pairs of edges sharing point 0 ($\omega \in [0^\circ, 90^\circ]$). The lengths of the edges are equal.

3.1. Stretching

Stretching is a common type of deviation from a uniformly-spaced mesh and it is readily defined for structured grids. In order to compare quadrilaterals and triangles in terms of sensitivity to stretching, the stretching type of mesh distortion is defined in a similar way as Fig. 5 depicts. In the quadrilateral case, the stretching is considered as the displacement of the edges sharing the center point 0 quantified by the stretching factors d_x and d_y. These edges are displaced in a structured way retaining their orientation, while stretching in the triangle case is defined via displacing the center node according to Fig. 5(b).

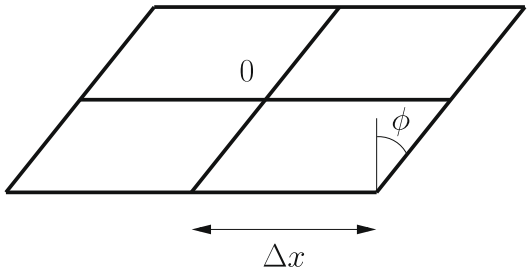

Fig. 7. *Sheared* mesh, depicting displacement of the edges causing deviation from orthogonality expressed by the angle $\phi(\phi \in [0^\circ, 90^\circ])$. The lengths of the edges are equal.

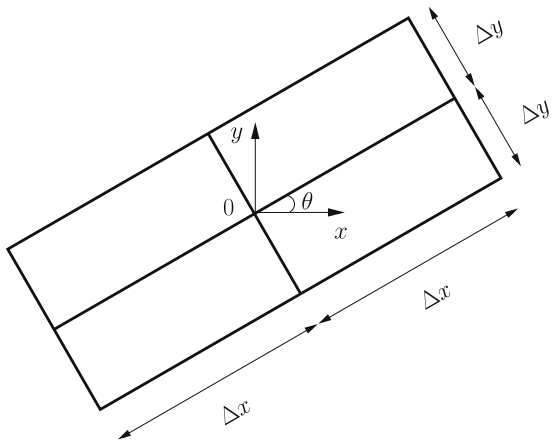

Fig. 8. *Rotated structured* mesh depicting non-alignment of the edges with the axes of the global system ($\Delta x \neq \Delta y$ and $\theta \in [0^\circ, 45^\circ]$).

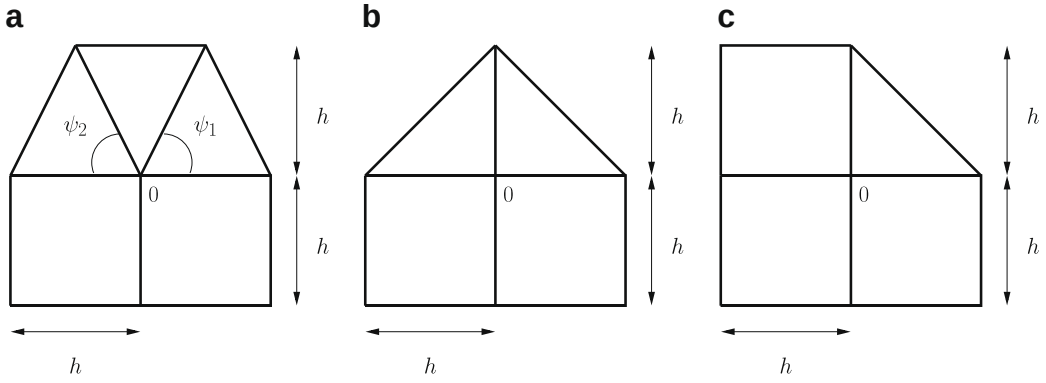

Fig. 9. Common *hybrid mesh interfaces*.

3.2. Skewness and shearing

The four edges sharing the center point 0 in a quadrilateral grid usually meet forming angles that deviate from 180° as Fig. 6 illustrates. This type of distortion is typically called *skewness*. The angle ω quantifies the degree of skewness and ranges from 0° to 90°. *Shearing* is quite different from skewness. It preserves the 180° angle between the edges and deviates the mesh from being orthogonal (Fig. 7). The angle ϕ quantifies this deviation and ranges from 0° to 90°. It will be seen that shearing and skewness affect the accuracy very differently.

3.3. Mesh rotation

Non-alignment of a structured mesh to a specific direction dictated by the form of the field is another type of distortion examined. The quadrilateral elements are rotated with respect to the x-axis of the coordinate system by an angle θ as illustrated in Fig. 8. This angle varies from 0° to 45°.

Table 1
Expressions for the error coefficients for each type of mesh distortion.

Mesh	e^x_{xy}	e^x_{xx}	e^x_{yy}	e^x_{xxx}	e^x_{yyy}	e^x_{xyy}	e^x_{xxy}
Fig. 5(a)	$\frac{1}{2}d_y\Delta y$	$d_x\Delta x$	0	$\neq 0$	0	$\neq 0$	$\neq 0$
Fig. 5(b)	$d_y h$	$d_x h$	0	$\neq 0$	0	$\neq 0$	$\neq 0$
Fig. 6	$\frac{3\sin(2\omega)\Delta x}{8\cos(\omega)+8}$	$\frac{[\cos(\omega)-1]\Delta x}{2}$	$\frac{[1-\cos(\omega)]\Delta x}{4}$	$\neq 0$	$\neq 0$	$\neq 0$	$\neq 0$
Fig. 7	0	0	0	$\neq 0$	0	$\neq 0$	$\neq 0$
Fig. 8	0	0	0	$\neq 0$	$\neq 0$	$\neq 0$	$\neq 0$

Table 2
Expressions for the error coefficients for the hybrid mesh interfaces.

Mesh	e^y_{xy}	e^y_{xx}	e^y_{yy}	e^y_{xxx}	e^y_{yyy}	e^y_{xyy}	e^y_{xxy}
Fig. 9(a)	0	$-\frac{h}{48}$	0	$\neq 0$	$\neq 0$	$\neq 0$	$\neq 0$
Fig. 9(b)	0	0	$-\frac{h}{10}$	0	$\neq 0$	$\neq 0$	$\neq 0$
Fig. 9(c)	$-\frac{h}{6}$	0	0	0	$\neq 0$	$\neq 0$	$\neq 0$

Table 3
Central interface point displacements for improving the accuracy of the u_y derivative evaluation for the hybrid mesh interfaces.

Mesh	Δx	Δy
Fig. 9(a)	non existent	non existent
Fig. 9(b)	0	$2(-10+3\sqrt{11})h$
Fig. 9(c)	$-\frac{h}{6}$	0

Table 4
Characteristic local lengths for the hybrid mesh interfaces.

Mesh	L_x	L_y
Mesh interface of Fig. 9(a)	$\frac{11}{12}h$	h
Mesh interface of Fig. 9(b)	h	h
Mesh interface of Fig. 9(c)	h	h

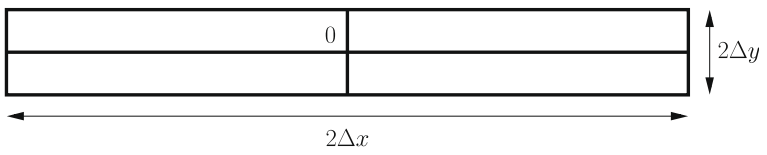

Fig. 10. High aspect ratio quadrilaterals typical of a structured mesh in a boundary layer region.

3.4. Hybrid mesh interfaces

Change in the topology of the elements creates special interfaces which require examination in terms of the local accuracy of the discretization [33]. The elements forming the interface (quadrilaterals and triangles) are considered to have the

Table 5
Mesh quality index Q expressions for the elementary types of mesh distortion.

Mesh	Q
Stretched structured Fig. 5(a)	$Q_x = \left\lvert \frac{d_x}{1+d_x^2} \right\rvert + \left\lvert \frac{d_y}{2+2d_y^2} \right\rvert$
Stretched unstructured Fig. 5(b)	Q_x Eq. (A-1)
Skewed Fig. 6	Q_x Eq. (A-2)
Sheared Fig. 7	$Q_x, Q_y = 0$
Non-aligned structured (Fig. 8)	$Q_x, Q_y = 0$
Mesh interface Fig. 9(a)	$Q_y = \frac{1}{44}$
Mesh interface Fig. 9(b)	$Q_y = \frac{144}{533}$
Mesh interface Fig. 9(c)	$Q_y = \frac{1}{6}$

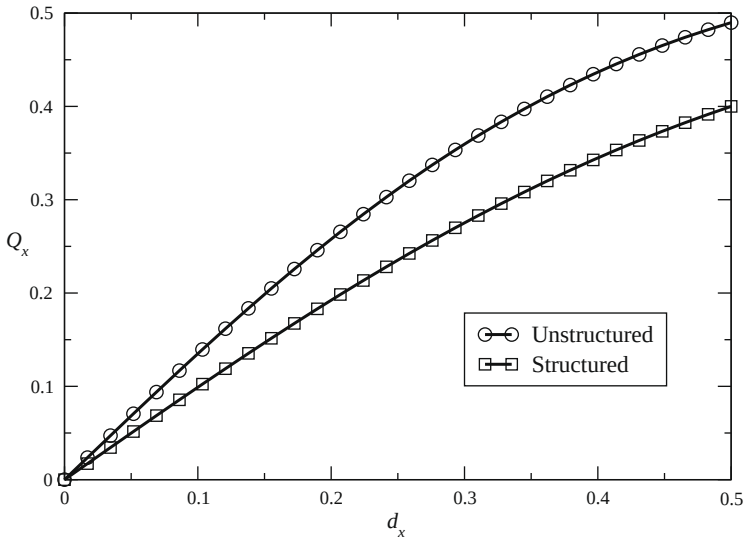

Fig. 11. Mesh quality index Q_x for the *stretched unstructured* mesh (○) and the *stretched structured* mesh (□) vs. displacement factor d_x ($d_y = 0$).

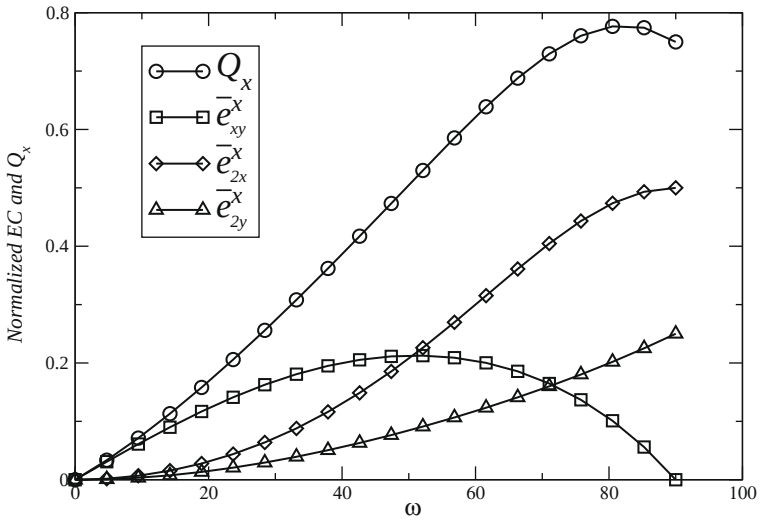

Fig. 12. Mesh quality index Q_x and its corresponding normalized error coefficients vs. the skewness angle ω.

same size so that the effect of the changing topology is isolated and studied. Three cases of such interfaces are identified in two dimensions and are illustrated in Fig. 9.

4. Direct relation between truncation error and mesh distortion

The general expressions of the *error coefficients* (EC) given in Eqs. (6) and (7) can yield simpler expressions *directly* related to each type of mesh distortion presented here. This is very important to subsequent work on improving the grid.

Table 1 gives the expressions of the EC for a mesh exhibiting only one type of distortion for each case (a row of the table). The related parameters d_x, d_y, ω are present in the expressions. For clarity of the table, the terms related to the higher order EC are not given, and it is just noted if they are zero or not. It is observed that stretching and skewness reduce the formal second order of the FV discretization to first. The error is proportional to the stretching parameters d_x and d_y. In the case of skewness, the relationship with ω is not linear. Finally, for the case of shearing and non-alignment of a structured mesh, no reduction of the order of accuracy occurs. However, the structure of the TE changes (terms $e^x_{xxx}, e^x_{yyy}, e^x_{xyy}$ and e^x_{xxy}) but the discretization remains second order.

The EC corresponding to evaluation of the derivative u_y of the three types of hybrid mesh interfaces are presented in Table 2. For the first type of interface, it is considered that $\psi_1 = \psi_2$. It is observed that mesh interfaces yield first order accuracy for the evaluation of the derivative u_y.

However, it is possible to relocate node 0, so that the order of accuracy of the u_y evaluation is improved, but only for the mesh interfaces of Figs. 9(b) and (c). In Table 3 the displacements of point 0 for improving the accuracy of the u_y evaluation are given. It should be noted that the results of Table 3 concern interfaces with equal "heights" (h) of the elements.

5. Definition of an appropriate index of mesh distortion

The focus of the present work is on *a priori* evaluation of a grid with regards to the shape and topology of its elements. The other aspect of grid quality, namely the local resolution is not addressed here. Therefore, the defined measure (index) of mesh distortion should be independent of the local size of the mesh. Other properties that this index should have include:

(1) simple mathematical form,
(2) direct relation with the TE, as well as the mesh distortion parameters,
(3) ability to capture distortions in any direction, and
(4) ability to detect relatively small distortions in the presence of larger ones.

5.1. Normalized error coefficients

The EC of Eqs. (6) and (7) are divided by the appropriate power of a characteristic local length scale L. Care must be taken in order to account for directionally-sized (high aspect ratio) local mesh elements. This implies appropriate use of two length scales (L_x, L_y) expressing the local size in the x- and y-direction, respectively.

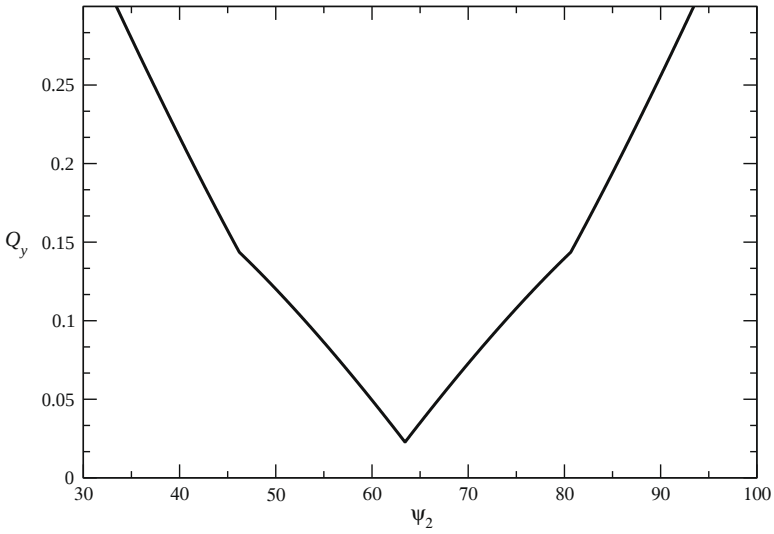

Fig. 13. Mesh quality index Q_y for the *hybrid mesh interface* of Fig. 9(a) vs. angle ψ_2.

The "normalized" EC of Eqs. (6) and (7) are defined as:

$$\overline{e^x}_{xx} = \frac{e^x_{xx}}{L_x}, \quad \overline{e^x}_{yy} = \frac{e^x_{yy}}{L_y}, \quad \overline{e^x}_{xy} = \frac{e^x_{xy}}{L_y}, \tag{20}$$

$$\overline{e^x}_{xxx} = \frac{e^x_{xxx}}{L_x^2}, \quad \overline{e^x}_{yyy} = \frac{e^x_{yyy}}{L_y^2}, \quad \overline{e^x}_{xxy} = \frac{e^x_{xxy}}{L_y^2}, \quad \overline{e^x}_{xyy} = \frac{e^x_{xyy}}{L_y^2}. \tag{21}$$

The denumerators in the above definitions have been chosen based on the mesh metrics appearing in the EC expressions and the order of each EC.

Carefull consideration is needed to define the characteristic local length. It is incorrect to define a single length for every direction, as then, on meshes with cells of high aspect ratio, the normalized EC would either be overestimated or underestimated. The present work uses an approach that resembles the FV evaluation of the derivative. It defines the following grid functions:

$$f_x = \Delta x_{e,k}|\Delta x_{e,k}|, \quad f_y = \Delta y_{e,k}|\Delta y_{e,k}|, \quad k = 1, 2. \tag{22}$$

Then, the lengths L_x, L_y are computed in a similar manner to Eq. (1) with u being replaced by f_x for the x-component and by f_y for the y-component:

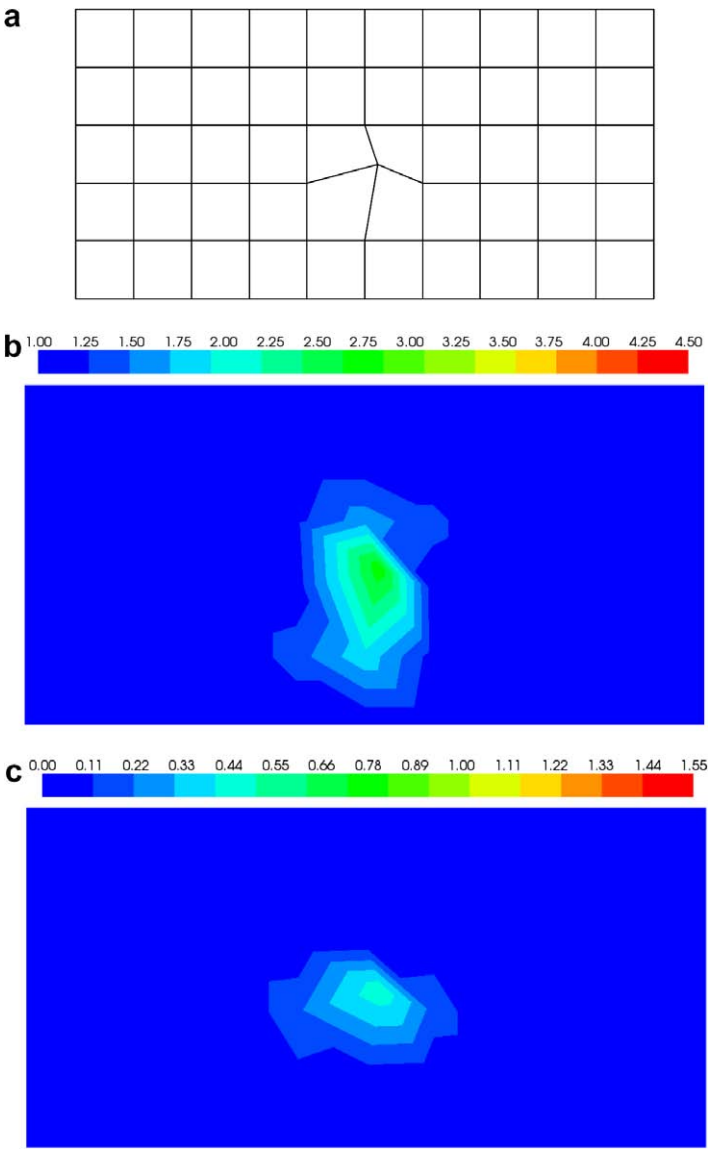

Fig. 14. Locally stretched *structured* channel mesh: (a) mesh geometry, (b) index q and (c) index Q.

$$L_x = \frac{1}{S}\sum_e f_{x,e}\Delta y_e, \quad L_y = -\frac{1}{S}\sum_e f_{y,e}\Delta x_e \tag{23}$$

It should be noted that for a uniform structured mesh with element sizes Δx and Δy, the characteristic lengths are:

$$L_x = \Delta x \quad \text{and} \quad L_y = \Delta y.$$

For the case of a uniform (honeycomb shape) triangular mesh of edge size h, the local lengths are:

$$L_x = \frac{35h}{48} \quad \text{and} \quad L_y = \frac{7\sqrt{3}h}{16}.$$

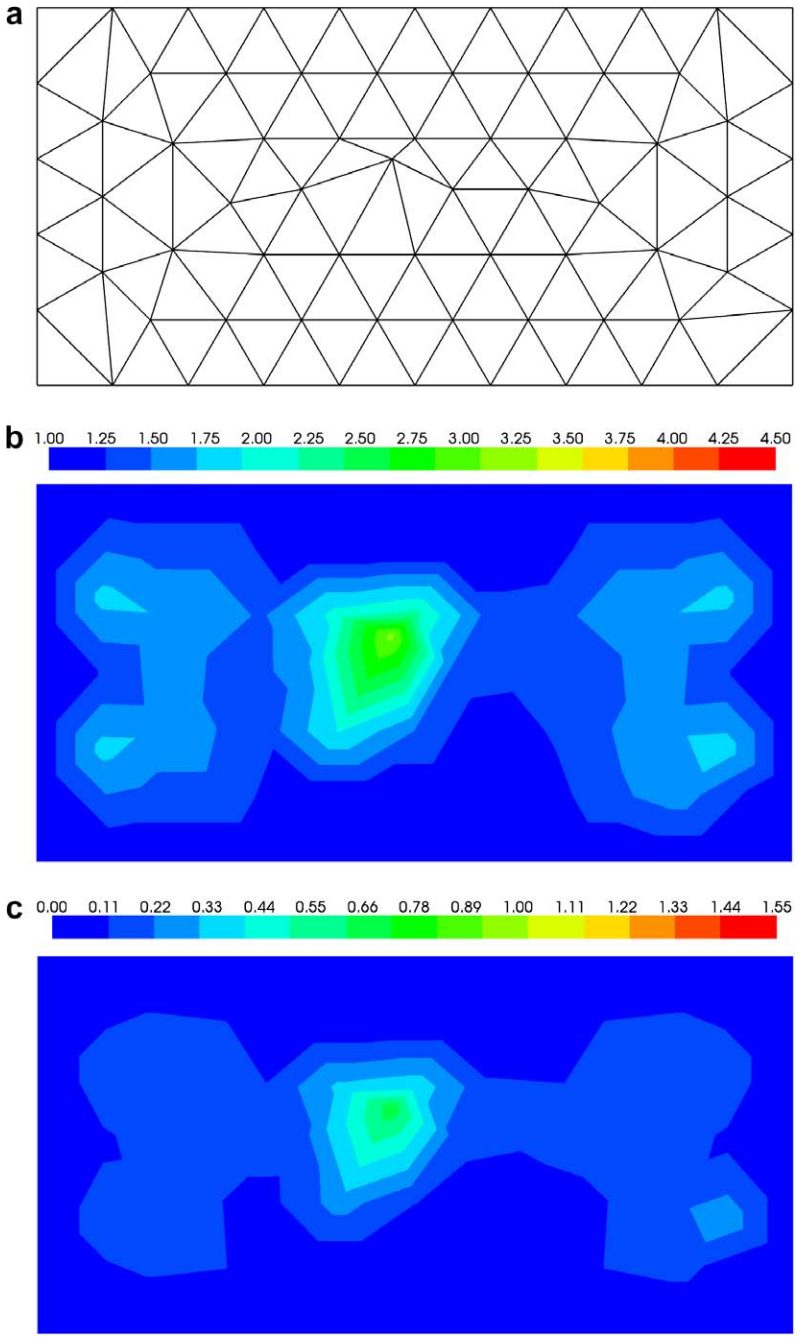

Fig. 15. Locally stretched *unstructured* channel mesh: (a) mesh geometry, (b) index q and (c) index Q.

Also, for the examined hybrid mesh interfaces the characteristic local lengths are given in Table 4.

5.2. Mesh quality index

The normalized EC are grouped to yield a single number that characterizes the quality of the grid. Two such groupings are being presented and evaluated.

The first is expressed via use of the first order error coefficients:

$$Q_x = |\overline{e^x}_{xx}| + |\overline{e^x}_{yy}| + |\overline{e^x}_{xy}|, \tag{24a}$$

$$Q_y = |\overline{e^y}_{xx}| + |\overline{e^y}_{yy}| + |\overline{e^y}_{xy}|. \tag{24b}$$

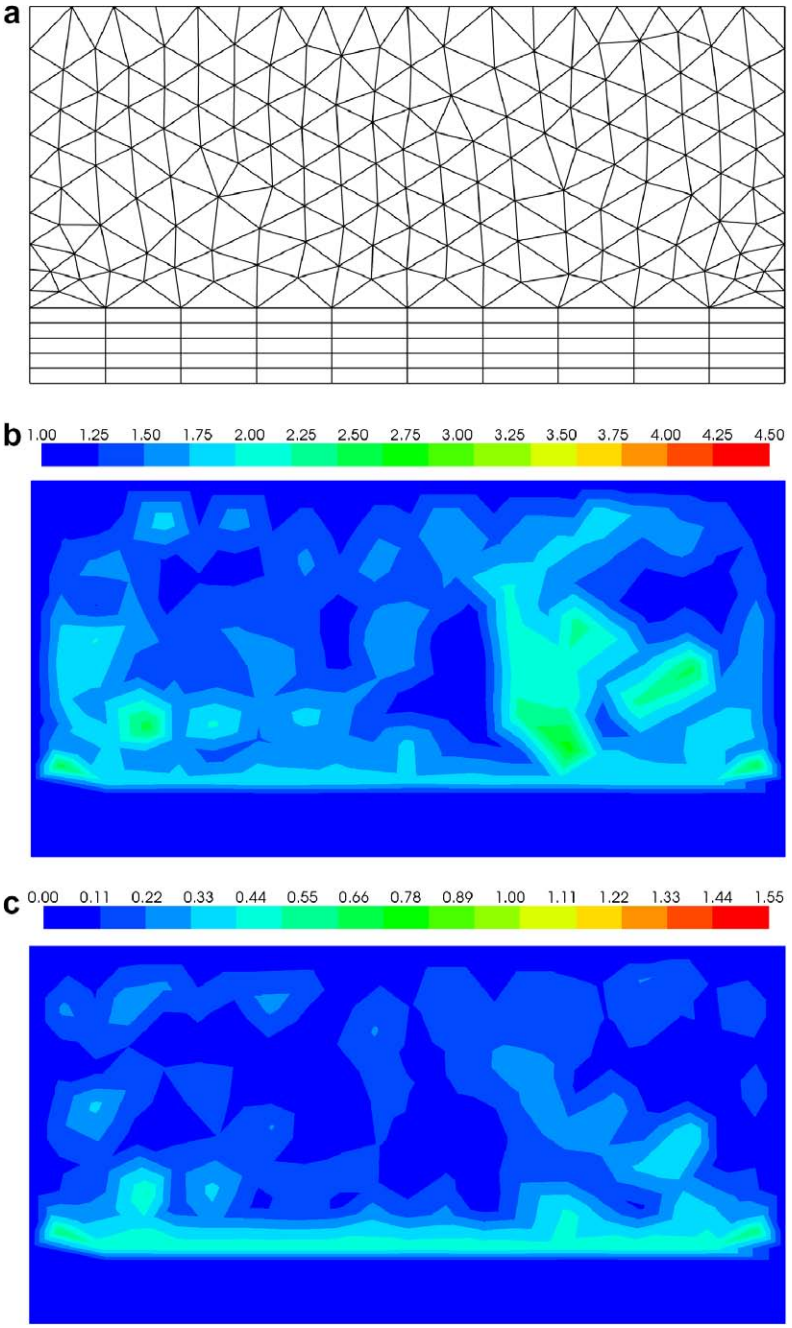

Fig. 16. *Hybrid* channel mesh: (a) mesh geometry, (b) index q and (c) index Q.

where the first expression regards the u_x-derivative evaluation, and the second concerns the u_y computation. On meshes which yield second order accuracy in the evaluation of the derivatives u_x and u_y, both Q_x and Q_y are equal to zero.

The second index that is presented expresses the *deviation* of a mesh from being ideal via the ratio of a form of the EC appearing on a general distorted mesh to a form of those coefficients for an ideal mesh. Specifically:

$$q_x = \frac{|\overline{e^x}_{xx}| + |\overline{e^x}_{yy}| + |\overline{e^x}_{xy}| + |\overline{e^x}_{xxx}| + |\overline{e^x}_{yyy}| + |\overline{e^x}_{xyy}| + |\overline{e^x}_{xxy}|}{|\overline{e^x}_{xxx}| + |\overline{e^x}_{xyy}|}, \tag{25a}$$

$$q_y = \frac{|\overline{e^y}_{xx}| + |\overline{e^y}_{yy}| + |\overline{e^y}_{xy}| + |\overline{e^y}_{xxx}| + |\overline{e^y}_{yyy}| + |\overline{e^y}_{xyy}| + |\overline{e^y}_{xxy}|}{|\overline{e^y}_{xxx}| + |\overline{e^y}_{xyy}|}. \tag{25b}$$

Index q *expresses the deviation of the mesh locally from being ideal*. It should be noted that q_x and q_y are equal to one for an ideal mesh, and have values greater than one for a general distorted grid.

It is interesting to examine the values of the indices for a structured mesh with high aspect ratio elements that is typical of boundary layer regions and illustrated in Fig. 10.

The relevant computation here is that of the derivative u_y. The relevant EC in Eq. (8) for this case are:

$$e^y_{xxy} = \frac{(\Delta x)^2}{8}, \quad e^y_{yyy} = \frac{(\Delta y)^2}{6},$$

which yields the mesh quality index Q_y to be zero and the q_y to be one, which are the best possible quality index values.

The experiment is repeated employing the triangular mesh created by subdividing the quadrilaterals of Fig. 10 along their diagonals. The corresponding error coefficients are:

$$e^y_{yyy} = \frac{(\Delta y)^2}{6}, \quad e^y_{xyy} = -\frac{\Delta x \Delta y}{6}, \quad e^y_{xxy} = \frac{(\Delta x)^2}{6}.$$

It is observed that the order of accuracy remains second ($Q_y = 0$). However, more non-zero EC appear and the value of q_y is not that of the ideal mesh, but is greater than one.

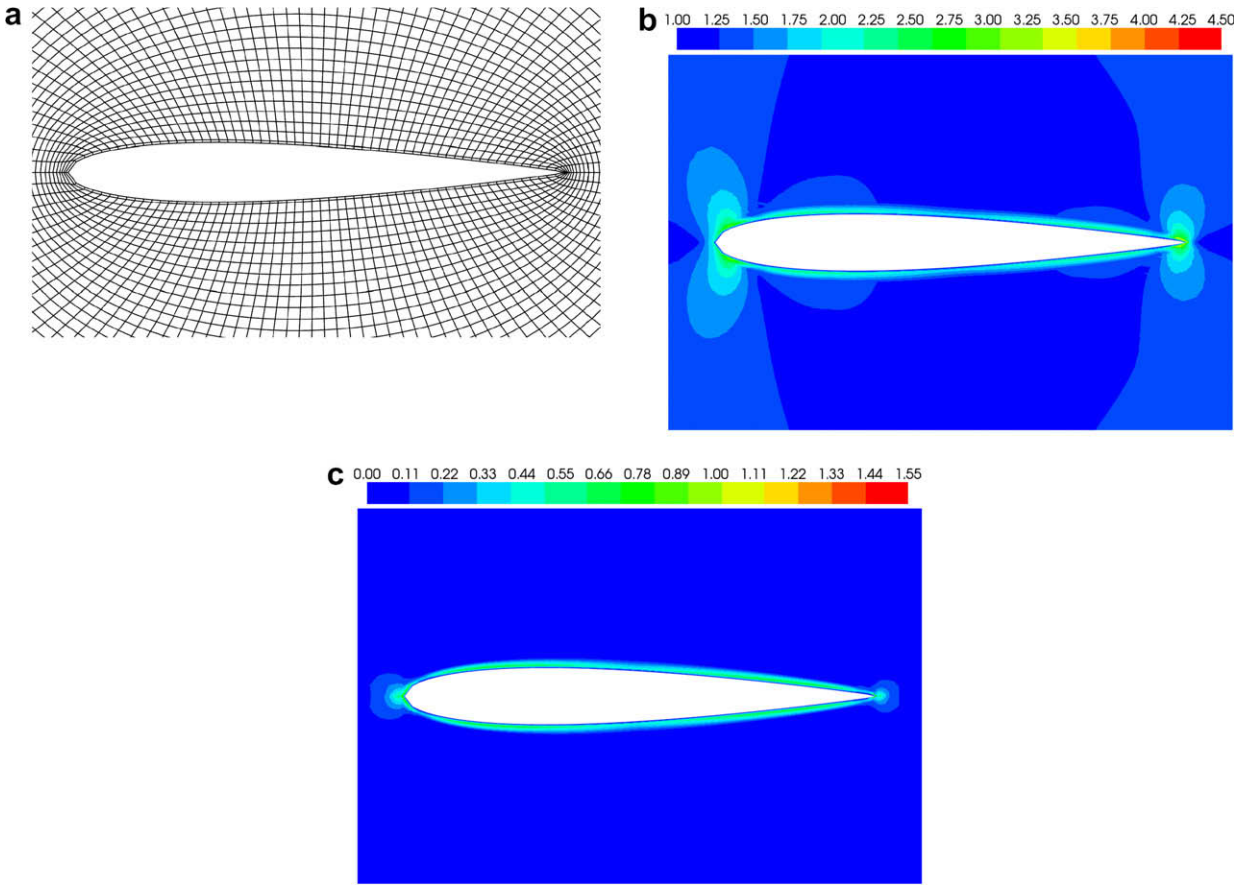

Fig. 17. O-type structured mesh around a NACA 0012 airfoil: (a) mesh geometry, (b) index q and (c) index Q.

5.3. Analytic expressions of the quality index Q for each type of elementary mesh distortion

The index Q has a simpler mathematical form and thus amenable to a *direct* relation to each type of mesh distortion. These expressions are given in Table 5. The equations for the stretched unstructured and the skewed structured mesh cases are given in Appendix A. It is observed that, the sheared and rotated (non-aligned) structured meshes do not exhibit reduction

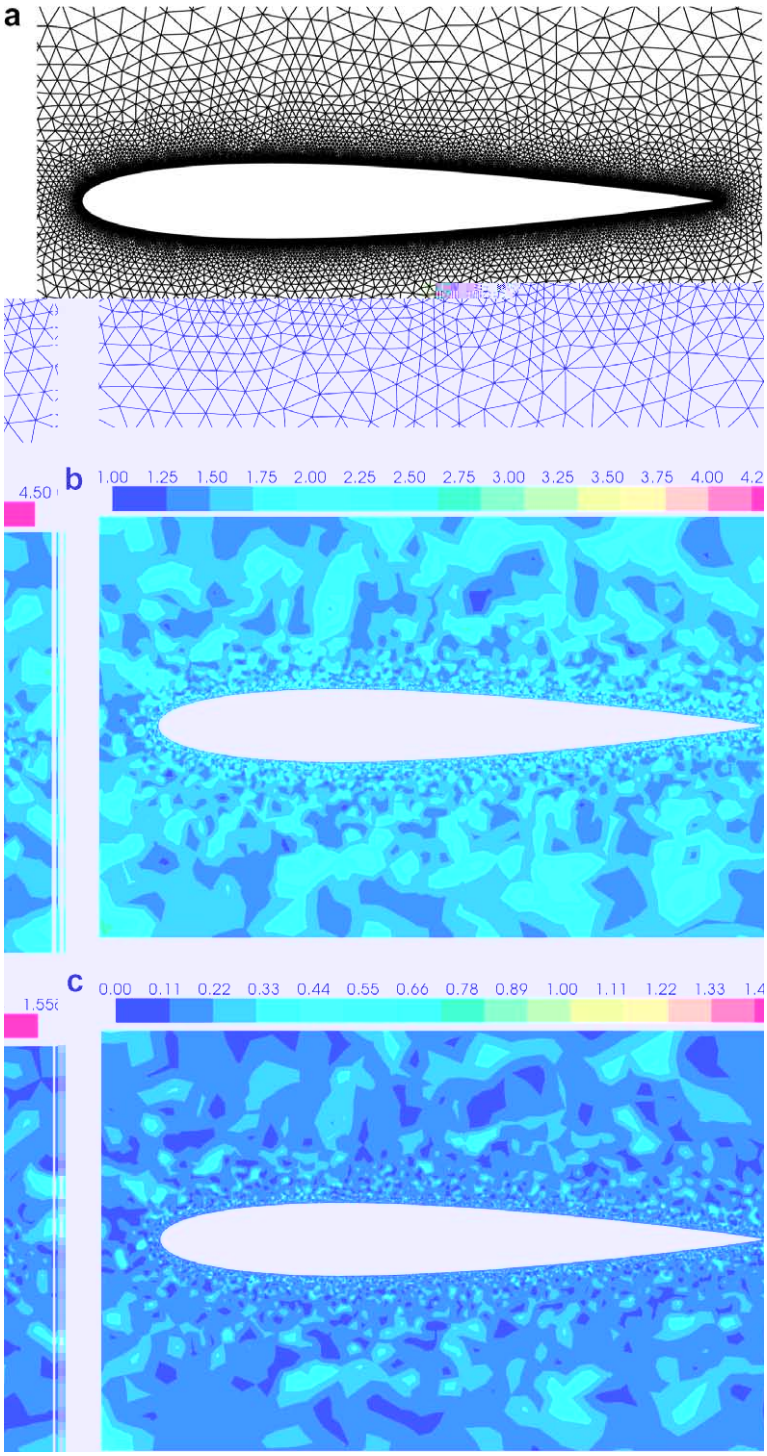

Fig. 18. Unstructured mesh around a NACA 0012 airfoil: (a) mesh geometry, (b) index q and (c) index Q.

of accuracy and thus the indices are equal to zero. The unstructured mesh exhibits higher sensitivity in mesh distortion as it is depicted graphically in Fig. 11. The variation of the index with respect to the skewness angle is given in the Appendix A, and it is shown graphically in Fig. 12. A peak in the degradation of accuracy is observed at about 80°. It is observed that the normalized error coefficient $\overline{e^x}_{xy}$ reduces as the skewness angle approaches 90°, which leads to the reduction of Q_x in the

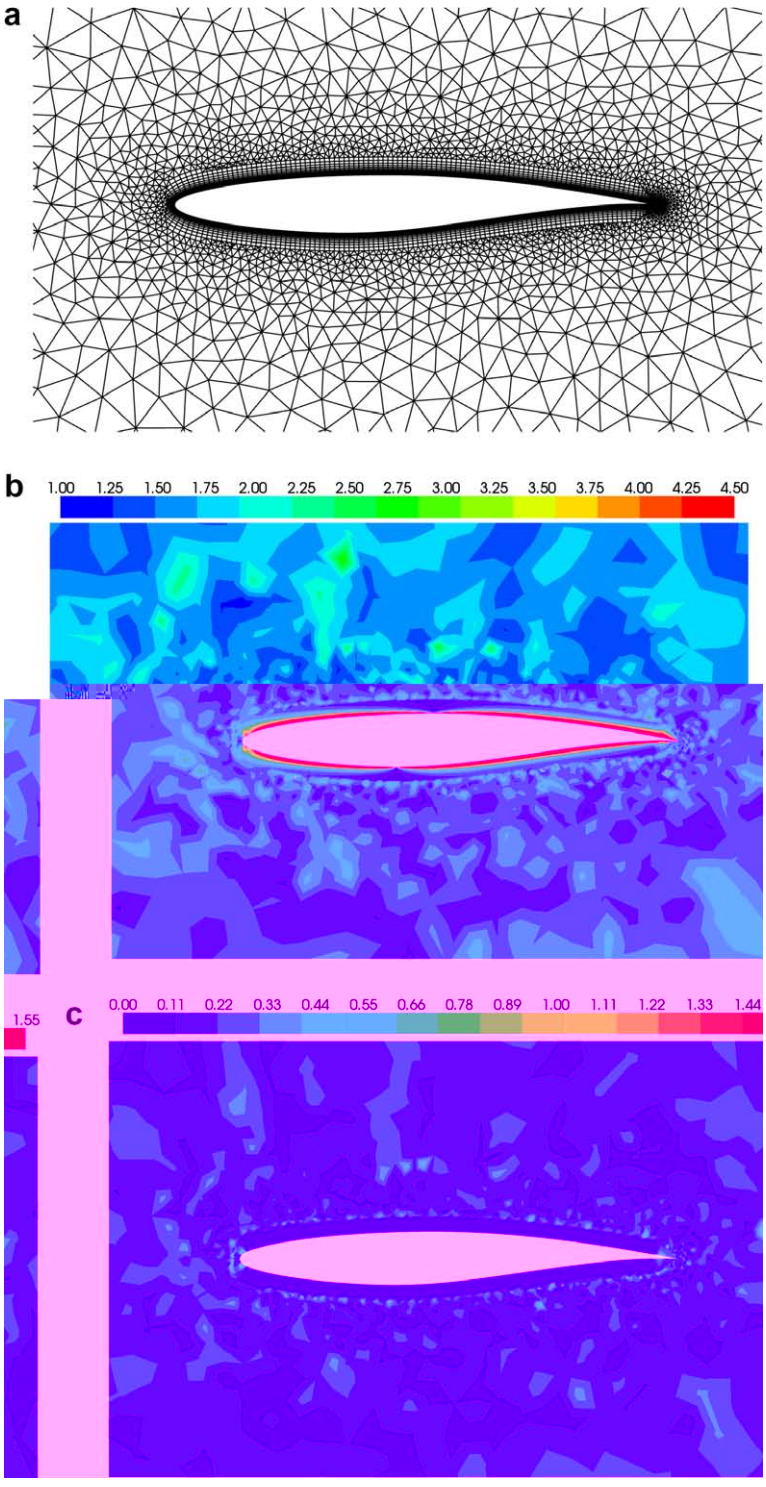

Fig. 19. Hybrid mesh around a RAE 2822 airfoil: (a) mesh geometry, (b) index q and (c) index Q.

same region in the graph. Finally, the influence of the mesh interface angle ψ_2 on degradation of accuracy is shown in the graph of Fig. 13. This concerns the hybrid mesh interface shown in Fig. 9(a). The curve is symmetric around the value of $\tan^{-1}(2) \approx 63^\circ$ for which Q_y is minimum.

5.4. Calibration of the mesh quality index Q

Any practical use of the grid quality index to judge a mesh requires knowledge of the range of permissible values of Q. A calibration is needed which is based on upper values of stretching d_x, d_y and skewness ω that are considered acceptable for typical field solvers. The proposed calibration has a conservative character as the upper bound for index Q is chosen as $max(Q_x, Q_y)$. An upper value of 20% stretching means a value of d_x and d_y of $\frac{1}{11}$, which when substituted in the expression for Q yields a value of approximately 0.13. Similarly for a maximum skewness angle ω of 20°, a value of $Q \approx 0.17$ is found.

Considering the case of a stretched unstructured mesh and applying the same stretching (center node displacement factor) of 20% a value of $Q \approx 0.24$ is found. Finally, for the hybrid mesh of Fig. 9(a), setting $\psi_2 = \tan^{-1}(2) \pm 20^\circ$ with $\psi_1 = 2 \cdot \tan^{-1}(2) - \psi_2$, an upper bound of $Q \approx 0.16$ is derived. Therefore, an upper bound value for Q of around 0.20 is a reasonable choice for all types of mesh distortion.

6. Application of the mesh quality indices

The quality index Q that is based on the first order error terms appears to be quite simpler to use compared to the index q that uses both the first and the second order terms. However, a decision to adopt Q cannot be made until both of them are implemented with general distorted meshes. This section employs three types of grids; structured, unstructured, as well as hybrid. The hybrid grids consist of separate quadrilateral and triangular layers, which is quite typical in applications. The

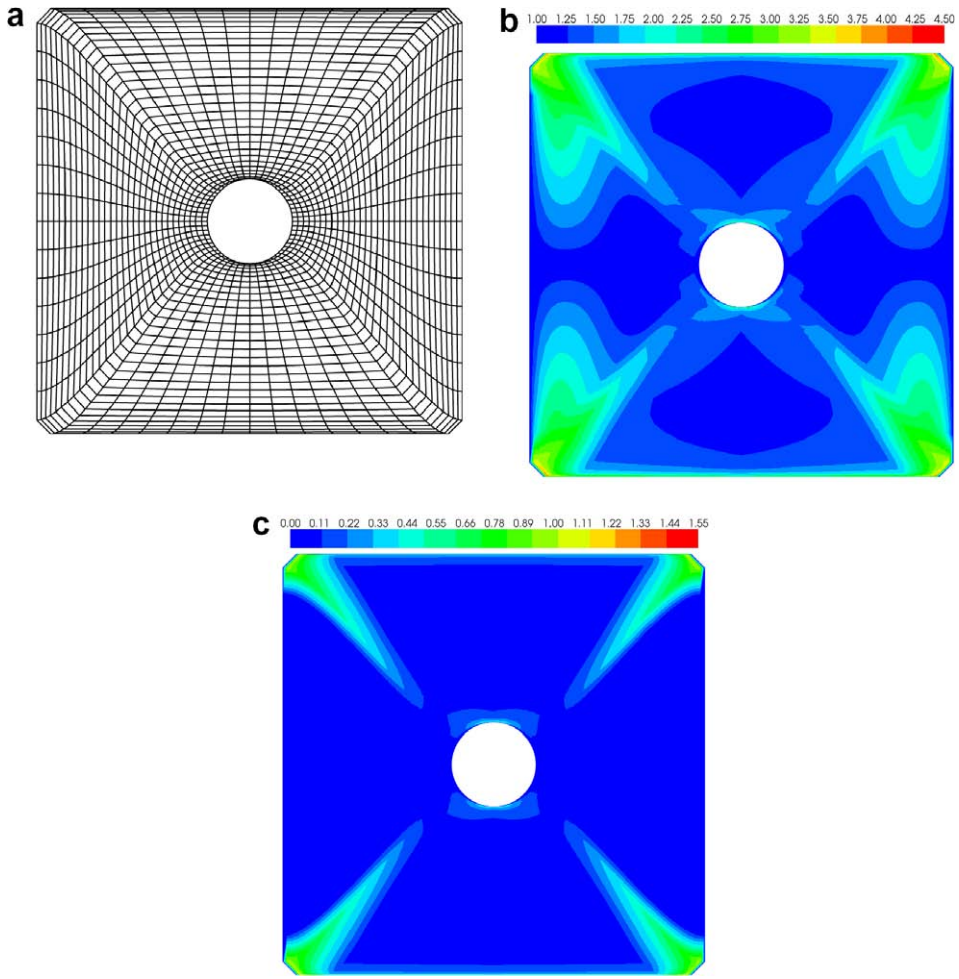

Fig. 20. Structured mesh around a cylinder: (a) mesh geometry, (b) index q and (c) index Q.

geometries involved are channel, airfoil and cylinder. It is important that the employed grids exhibit (i) both small and large magnitude distortions, as well as (ii) local and more global ones. The contours of the functions $Q \equiv max(Q_x, Q_y)$ and $q \equiv max(q_x, q_y)$ are plotted for all cases.

In order to compare the effectiveness–fidelity of the indices for the different cases, the same contour levels are plotted, that is the minimum, maximum and number of levels are the same for all grids for each index. Further, both indices (Q and q) are shown with the same number of contour levels, which is essential for comparing the two on the same mesh.

6.1. Channel grids

The structured channel grid shown in Fig. 14 is uniform everywhere except in the middle where a point is displaced. Both indices capture this distortion with index Q-contours being more focused. The same displacement is applied to an almost uniform triangular mesh shown in Fig. 15. Similarly here, both indices capture the primary distortion along with smaller ones with q capturing a bit broader area than Q. This is due to the second order EC included in the definition of index q.

The third mesh is hybrid with a straight line transitioning from the quadrilaterals to the triangles shown in Fig. 16. The index Q is more focused on the interface region than index q does.

6.2. Airfoil grids

An O-type structured mesh for the NACA 0012 airfoil is employed next. There is a sudden expansion of the quadrilaterals size in the region close to the surface as shown in Fig. 17. The same observation is made here, namely Q captures the areas of mesh stretching and skewness (leading and trailing edge regions) stronger compared to index q.

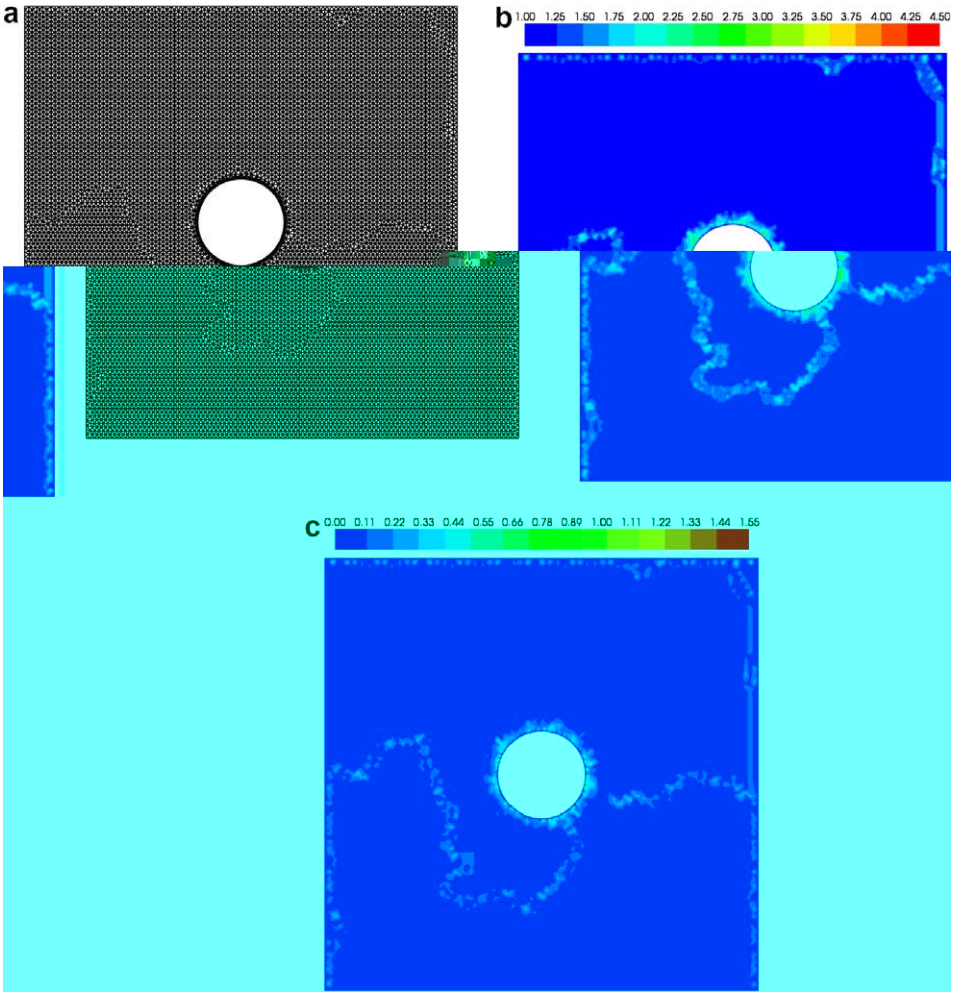

Fig. 21. Unstructured mesh around a cylinder: (a) mesh geometry, (b) index q and (c) index Q.

The unstructured mesh around the NACA 0012 shown in Fig. 18 is a good quality mesh with small distortions everywhere. This case was devised to check the indices' sensitivity to relatively small ("background") distortions. It is observed that both indices show sensitivity to these non-uniformities with q being more sensitive to them.

Finally, a hybrid mesh around the RAE 2822 airfoil is employed (Fig. 19). This is a viscous mesh with a very good preservation of the order of accuracy in the boundary layer region, except at the mesh interfaces, as indicated by index Q. However, index q shows a large deviation from the ideal computation for the boundary layer region due to the non-alignment of the structured mesh in that area with the axes of the system of reference.

6.3. Cylinder grids

The cylinder mesh has mild distortions away from the body surface. It is an interesting case to check the performance of the quality indices at the farfield. Fig. 20 illustrates the structured mesh which exhibits skewness along lines "diagonally" off the surface. The grid is of good quality close to the cylinder and this is indicated by both indices. It is observed that the four "skewness lines" are captured more clearly by index Q.

The next case involves a triangular grid exhibiting a large stretching area close to the surface, as well as a mild mesh distortion of irregular shape away from the cylinder (Fig. 21). The two indices do recognize both types of distortion, and their contours "follow" the mild distortion pretty closely.

Finally, the hybrid grid of Fig. 22 exhibits irregularity of the interface between the quadrilaterals and the triangles, as well as quite strong distortions in the farfield. It is observed that both indices recognize both types of strong distortions; the circular-shaped interface and the "random" ones in the triangles zone.

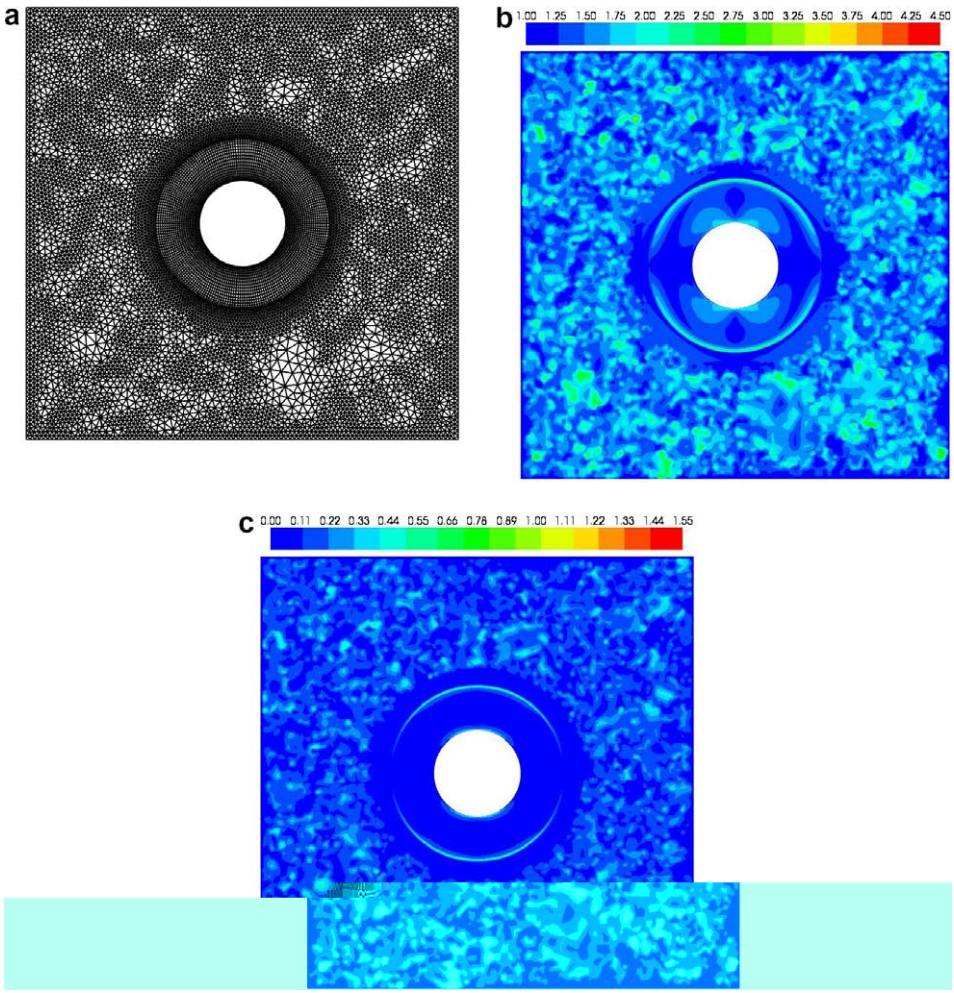

Fig. 22. Hybrid mesh around a cylinder: (a) mesh geometry, (b) index q and (c) index Q.

7. Summary

The present work developed and evaluated *a priori* indicators of mesh distortion. This was accomplished by deriving the *complete* truncation error expression for the Finite Volume discretization of the field gradient in two dimensions. The complexity of the mathematical operations involved was overcome via use of symbolic mathematics software.

The presented work analyzed a generally-distorted mesh (structured, unstructured and hybrid) into elementary distortions (stretching, skewness, shearing, rotation), as well as three common types of interfaces, and those were *directly* related to the TE. The derived analytic expressions are relatively simple and amenable to future work on improving the mesh. This is especially true for index Q for which analytic expressions were presented *directly* relating it to the degree of stretching and skewness, as well as to hybrid mesh interfaces.

The two indices (Q and q) "followed" the grid distortion quite faithfully with Q being more focused on these local areas. Index q marks broader areas of the mesh due to the second order error terms included in its definition. It also picks-up small (background) distortions which may not be of interest. Given the fact that Q is quite simpler to calculate, it is the recommended quality index. A disadvantage of Q is that it cannot indicate the quality of distorted meshes that still yield second order accurate computation of the gradient. Shearing and rotation do change the TE (i.e. only index q "picks them" up) but they do not reduce the order of accuracy. However, the goal is to fix meshes that degrade the accuracy to a lower order.

The following observations were also made for both indices: (i) irregularly-shaped small distortions were captured faithfully, (ii) small distortions were detected even though much larger ones existed in the mesh, and (iii) distortions were captured in any direction.

Employment of the *centroid* dual discretization must be avoided on general structured and hybrid meshes due to its inconsistency in the evaluation of the field gradient.

Future work involves two directions: (i) working the analytical expressions for the three-dimensional case for hybrid (structured/unstructured) grids, and (ii) using the analytic expressions of the present work for *a priori* improvement of the mesh.

Appendix A

Mesh quality index Q_x for the *stretched unstructured* mesh of Fig. 5(b):

$$Q_x = \frac{96}{7}\left|\frac{dx}{|1+2dx|(1+2dx)+4(1+dx^2)+|2dx-1|(1-2dx)}\right| + \frac{32}{7}\sqrt{3}\left|\frac{dy}{(2dy-\sqrt{3})[|2dy-\sqrt{3}|+|\sqrt{3}+2dy|]+2dy}\right|. \tag{A-1}$$

Mesh quality index Q_x for the *skewed* mesh of Fig. 6:

$$Q_x = \frac{1-\cos^2(\omega)}{2[\cos^2(\omega)+1]} + \frac{\cos(\omega)-1}{\cos^2(\omega)-\cos(\omega)-4} - \frac{3\sin(2\omega)}{2[\cos(\omega)+1][\cos^2(\omega)-\cos(\omega)-4]}. \tag{A-2}$$

References

[1] Y. Kallinderis, Hybrid grids and their applications, Handbook of Grid Generation, CRC Press, Boca Raton, FL, 1999 (Chapter 35).
[2] T. Baker, Adaptive modification of time evolving meshes, Computer Methods in Applied Mechanics and Engineering 194 (2005) 4977–5001.
[3] H. Jasak, A. Gosman, Automatic resolution control for the finite-volume method, Parts 1,2, and 3, Numerical Heat Transfer 38 (2000) 237–290.
[4] H. Jasak, A. Gosman, Element residual error estimate for the finite-volume method, Computers and Fluids 32 (2003) 223–248.
[5] D. McRae, r-Refinement grid adaptation algorithms and issues, Computer Methods in Applied Mechanics and Engineering 189 (2000) 1161–1182.
[6] Y. Kallinderis, Grid adaptation by redistribution and local embedding, VKI Lecture Series (1996).
[7] J.M. Escobar, R. Montenegro, G. Montero, E. Rodriguez, J. Gonzalez-Yuste, Smoothing and local refinement techniques for improving tetrahedral mesh quality, Computers and Structures 83 (2005) 2423–2430.
[8] R.V. Garimella, M.J. Shashkov, P.M. Knupp, Triangular and quadrilateral surface mesh quality optimization using local parametrization, Computer Methods in Applied Mechanics and Engineering 193 (2004) 913–928.
[9] J. Dompierre, M.G. Vallet, P. Labbé, F. Guibalt, An analysis of simplex shape measures for anisotropic meshes, Computer Methods in Applied Mechanics and Engineering 194 (2005) 4895–4914.
[10] Y. Kallinderis, S. Kwong, Viscous Grids and Assessment of their Quality, in: 15th AIAA Computational Fluid Dynamics Conference, AIAA-2001–2539, 2001.
[11] P.M. Knupp, Algebraic mesh quality metrics for unstructured initial meshes, Finite Elements in Analysis and Design 39 (2003) 217–241.
[12] J.C. Tannehill, D.A. Anderson, R.H. Pletcher, Computational Fluid Mechanics and Heat Transfer, second ed., Series in Computational and Physical Processes in Mechanics and Thermal Sciences, Taylor and Francis, 1997.
[13] B. Ataie-Ashtiani, S. Hosseini, Error analysis of finite difference methods for two-dimensional advection-dispersion-reaction equation, Advances in Water Resources 28 (2005) 793–806.
[14] S. Sankaranarayanan, M.L. Spaulding, A study of the effects of grid non-orthogonality on the solution of shallow water equations in boundary-fitted coordinate systems, Journal of Computational Physics 184 (2003) 299–320.
[15] D. You, R. Mittal, M. Wang, P. Moin, Analysis of stability and accuracy of finite-difference schemes on a skewed mesh, Journal of Computational Physics 213 (2006) 184–204.
[16] T. Ikeda, P. Durbin, Mesh stretch effects on convection in flow simulations, Journal of Computational Physics 199 (2004) 110–125.
[17] J. Thompson, Numerical Grid Generation, North-Holland, New York, 1982.

[18] M.B. Giles, Accuracy of node-based solutions on irregular meshes, in: D.L. Dwoyer, M.Y. Hussaini, R.G. Voigt, D.L. Dwoyer (Eds.), 11th International Conference on Numerical Methods in Fluid Dynamics of Lecture Notes in Physics 323 (1989) 273–277.
[19] Y.N. Jeng, J.L. Chen, Truncation error analysis of the finite volume method for a model steady convective equation, Journal of Computational Physics 100 (1992) 64–76.
[20] E. Turkel, Accuracy of schemes with nonuniform meshes for compressible fluid flows, Applied Numerical Mathematics 2 (1986) 529–550.
[21] Matlab, Symbolic Math Toolbox, The Matlab Inc., 1998.
[22] M.J. Berger, P. Collela, An adaptive multigrid method for the euler equations, Lecture Notes in Physics 218 (1985) 92–97.
[23] M.J. Berger, P. Collela, Local adaptive mesh refinement for shock hydrodynamics, Journal of Computational Physics 82 (1989) 64–84.
[24] C. Ilinca, A comparison of three error estimation techniques for finite-volume solutions of compressible flows, Computer Methods in Applied Mechanics and Engineering 189 (2000) 94–121.
[25] M. Thompson, An adaptive multigrid technique for the incompressible Navier–Stokes equations, Journal of Computational Physics 82 (1992) 94–121.
[26] Y. Kallinderis, J. Baron, A new adaptive algorithm for turbulent flows, Journal of Computers and Fluids 21 (1992) 77–96.
[27] M. Ainsworth, J.T. Oden, A Posteriori Error Estimation in Finite Element Analysis, Wiley-Interscience, New York, 2000.
[28] J.T. Oden, I. Babuska, F. Nobile, Y. Feng, R. Tempone, Theory and methodology for estimation and control of errors due to modelling, approximation and uncertainty, Computer Methods in Applied Mechanics and Engineering 194 (2005) 195–204.
[29] S. Prudhomme, J.T. Oden, On goal-oriented error estimation for elliptic problems: application to the control of pointwise errors, Computer Methods in Applied Mechanics and Engineering 176 (1999) 313–331.
[30] S. Prudhomme, J.T. Oden, A posteriori error estimation in fluid mechanics, in: Proceedings of the Finite Elements in Flow Problems 2000 Conference, The University of Texas at Austin, April 30–May 4, 2000.
[31] T.J. Barth, Aspects of unstructured grids and finite volume solvers for the euler and Navier–Stokes equations, VKI Lecture Series (1995).
[32] C. Hirsch, Numerical computation of internal and external flows, Fundamentals of Numerical Discretization, 1, John Wiley and Sons, 1988.
[33] Y. Kallinderis, Numerical treatment of grid interfaces for viscous flows, Journal of Computational Physics 98 (1992) 129–144.